$+1$ for $\theta < 0$

(x^-) = vector of mole fractions in the reservoir at $z = -1$ for $\theta < 0$

(y) = $(x) - (x^+)$ for the nonflow diffusion tube or $(x) - (x^0)$ for the tubular reactor

$\bar{y}$ = mole fraction integrated over tube length

z = z^*/L (nonflow) or $z^* D_R/V_m R^2$ (tubular reactor) = axial coordinate, dimensionless

z^* = axial coordinate, cm.

Greek Letters

α = $x^- - x^+$

η = radial position in tubular reactor, dimensionless

θ = $t\, D_R/L^2$ = time, dimensionless

λ = eigenvalue

ω_p = defined by Equation (4*b*)

Ω_p = defined by Equation (4*a*)

LITERATURE CITED

1. Bak, Thor A., "Contributions to the Theory of Chemical Kinetics," W. A. Benjamin, New York (1963).
2. Bischoff, Jerry R., and David M. Mason, *Chem. Eng. Sci.*, **23**, 447 (1968).
3. Bodenstein, Max, *Z. Phys. Chem.*, **29**, 295 (1899).
4. Bray, William C., *J. Am. Chem. Soc.*, **43**, 1262 (1921).
5. Bray, William C., and Kerman A. Liebhafsky, *ibid.*, **53**, 38 (1931).
6. Christiansen, J. A., *Z. Elektrochemie*, **62**, 225 (1958).
7. Gmitro, John I., and L. E. Scriven, "Symposium of the International Society for Cell Biology," Vol. V, p. 221, Academic Press, New York (1966).
8. Higgins, Joseph, *Ind. Eng. Chem.*, **59**, 18 (1967).
9. Kim, Young Gul, *Chem. Eng. Sci.*, **23**, 687 (1968).
10. Lefever, R., G. Nicolis, and I. Prigogine, *J. Chem. Phys.*, **47**, 1045 (1967).
11. Lotka, Alfred J., *J. Phys. Chem.*, **14**, 271 (1910).
12. ———, *J. Am. Chem. Soc.*, **42**, 1595 (1920).
13. Moore, Margaret J., *Trans. Faraday Soc.*, **45**, 1098 (1949).
14. Othmer, H. G., and L. E. Scriven, paper presented at 35th Ann. Chem. Eng. Symp., A.C.S., Illinois Inst. Tech., Chicago (Dec. 1968).
15. Prigogine, I., "Introduction to the Thermodynamics of Irreversible Processes," 3rd edit., Interscience, New York (1967).
16. ———, and R. Lefever, *J. Chem. Phys.*, **48**, 1695 (1968).
17. Prigogine, I., and G. Nicolis, *ibid.*, **46**, 3542 (1967).
18. Rinker, Robert G., Scott Lynn, David M. Mason, and William H. Corcoran, *Ind. Eng. Chem. Fundamentals*, **4**, 282 (1965).
19. Shaw, D. H., and H. O. Pritchard, *J. Phys. Chem.*, **72**, 1403 (1968).
20. Solomon, Robert Lee, Ph.D. thesis, Univ. Illinois, Urbana (1969).
21. ———, and J. L. Hudson, *AIChE J.*, **17**, 371 (1971).
22. Sullivan, John H., *J. Chem. Phys.*, **46**, 73 (1967).
23. Toor, H. L., *Chem. Eng. Sci.*, **20**, 941 (1965).
24. Turing, A. M., *Phil. Trans. Roy. Soc.*, **237**, 37 (1952).

Manuscript received April 24, 1969; revision received February 24, 1970; paper accepted March 2, 1970.

Analysis of Flow Choking of Two-Phase, One-Component Mixtures

W. J. KLINGEBIEL and R. W. MOULTON

University of Washington, Seattle, Washington

The nature of flow choking has been studied as steam-water mixtures are passed through a tube with ever increasing pressure gradient. Choked flow for two-phase, one-component mixtures has been characterized with a separated flow model as resulting from maximization of the ratio of gas to liquid velocities, or slip ratio. Slip ratios at choking were measured and found to increase from 1.2 to 5.0 at 30 lb./sq.in. exit plane pressure with decrease in quality from 0.95 to 0.02. Separated models predict either 9.3 or 28.4 with no quality dependence. The difference is attributed to liquid entrainment. Flow regimes were observed to vary from purely entrained to annular entrained to slug entrained as quality decreased. Normal shock waves were observed in the free jet at qualities above 0.25. Choking flow rates were predicted with an average error of less than 2% with a stagnation energy balance model using an empirically developed slip ratio relation corrected for entrainment.

High-velocity flow of vapor-liquid mixtures through ducts is characterized by ill-defined interfaces between phases and momentum and thermal relaxation times sufficiently long to result in nonequilibrium flow. Improved characterization of such a complex flow system has been the goal of researchers working in such diverse fields as oil reservoir recovery, rocket engine design, and nuclear reactor cooling. Of particular interest has been the prediction of choking conditions under which further increases in flow rate through a duct cannot be produced by decreasing downstream pressure.

Historically, choking, or critical flow, in a two-phase system was first analyzed by assuming that the two phases

W. J. Klingebiel is with Union Carbide, Bound Brook, New Jersey.

made up a homogeneous compressible fluid (*1* to *4*). The maximum flow rate at choking was then given by $G_c = \sqrt{-g_c\left(\frac{dP}{dV_m}\right)}$, where V_m is a mass averaged volume. However, fluid flow rates were experimentally measured and found to be as much as six times greater than homogeneous model predictions (*5*). Reasons for this have been suggested but incorporating them into analytical models has been a difficult proposition. Acceleration of the gas past the liquid and concentration of the more dense phase near the wall of the conduit have been suggested as possible mechanisms leading to higher flow rates than the homogeneous model predicts (*6*). Acceleration in a constant-diameter tube also can be shown to produce a departure from thermodynamic equilibrium; momentum, mass, and energy transport all have characteristic relaxation times and the exposure time afforded adjacent phases may not be sufficient for equilibrium conditions to exist.

Attention in recent years has concentrated on a separated flow model which characterizes choking as a maximization in the slip of the gas phase past a separate liquid phase. The effect of an average velocity difference between phases or slip on choking flow rates has been predicted analytically by several different separated flow models (*1*, *7* to *9*). However, no one has verified experimentally the values for slip used in these models. This study was designed to assess experimentally the slip contribution. In the course of this study the nature of two-phase choking and the validity of a separated flow model description were experimentally studied. Variations in pressure profiles, quality, mass flow rate, slip ratio, and flow patterns were followed as pressure gradient across the test section was incrementally increased.

DESCRIPTION OF EXPERIMENTAL SETUP

The basic supply system for the two-phase, steam-water choking studies conducted is shown in Figure 1. Metered streams of steam and water were mixed, passed through a precisely machined 0.504-in. I.D. stainless steel tube 22 in. long, discharged into a large plenum chamber, and then condensed and passed to a sewer. The thrust of the two-phase mixture leaving the test section was measured with an impulse cage-load cell arrangement. Pressure profiles were measured both in the test section and downstream in the freely expanding jet. The plenum was also removed in order to observe flow patterns and the free jet.

The static pressure profile within the test section was measured with 10 0.025-in. diam. taps drilled at precisely located positions along the tube using methods described in reference *15*. To this was added via electro-discharge machining a single 0.005 ± 0.0005-in. diam. tap with a center line 0.005-in. from the exit plane of the test section. Two pressure probes shown in reference *15* were used as well to measure the radial variation in static pressure near the tube exit and to characterize the axial pressure profile of the freely expanding jet. Probe 1, which could be positioned using a vernier traversing mechanism with an accuracy of ± 0.005 in., was streamlined and used to study the free jet and to show that the presence of a momentum cage had no choking effect on the flow from the test section. This probe was made of thick walled, ⅛-in. O.D. stainless steel tubing with a single 0.0125-in. tap. Probe 2 was also made of ⅛-in. O.D. thick-walled stainless tubing, but was constructed like a trombone so that thermal expansion effects could be minimized. Three 0.005-in. diam. pressure taps separated 120 deg. from each other on the same longitudinal plane were formed in this probe also using the electro-discharge machining technique. The estimated maximum error in radial-axial positioning with this probe was ± 0.001 in. It was used to compare probe and wall static pressure values near the exit plane of the test assembly. A flexible static probe made of ¼-in. copper tube with a single 0.0125-in. diam. tap was used to define the static pressure field throughout the plenum chamber interior during flow tests.

THRUST MEASUREMENT

The separated flow model requires some value for slip ratio k in order to characterize a particular flow situation. A value for the separated flow slip ratio can be found by measuring the thrust of the two-phase jet if the frictional resistance of the surrounding fluid can be neglected. The force balance used to measure the jet impulse is illustrated in Figure 2. The exterior of the impulse cage was taken as the control volume for the force balance. This impulse cage was so designed that all flow left in a radial direction and all secondary flow induced by the expanding jet entered the control volume radially. This last point was repeatedly verified with pressure probe traverses of the plenum chamber during operation.

Since primary flow is assumed to enter parallel to the longitudinal axis and leave perpendicular to it, a longitudinal force balance over the indicated control volume yields

$$\frac{1}{g_c}(wv)_e + P_eA_e = F + P_RA_R - P_R(A_R - A_e) \qquad (1)$$

Using the two-phase, separated flow relations one obtains

$$F + A_e(P_R - P_e) = \frac{1}{g_c}A_eG^2\left[x^2v_g + k(1-x)xv_f + \frac{x(1-x)v_f}{k} + (1-x)^2v_f\right] \qquad (2)$$

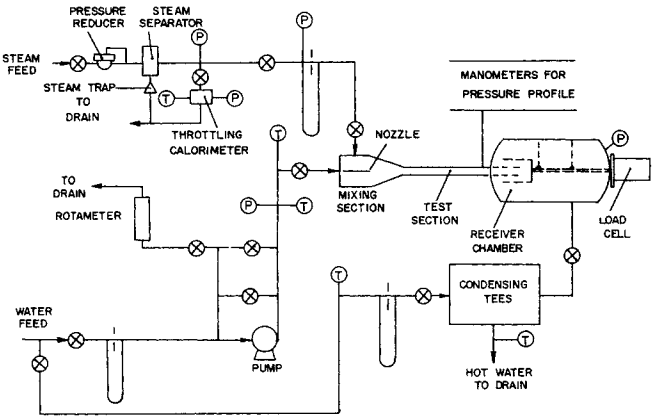

Fig. 1. Schematic diagram of apparatus.

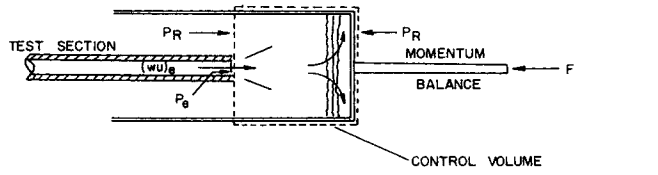

SLIP RATIO - QUALITY

$$\frac{1}{g_0}(WU)_e + P_eA_e = F + P_rA_r - P_r(A_r - A_e)$$

$$F + A_e(P_r - P_e) = \frac{A_e}{g_c}G^2\left[X^2V_g + K(1-X)XV_f + \frac{X(1-X)V_f}{K} + (1-X)^2V_f\right]$$

$$H = Xh_g + (1-X)h_f + \frac{1}{2g_cJ}\left[XU_g^2 + (1-X)U_f^2\right]$$

Fig. 2. Control volume for momentum measurement.

Solving for slip ratio, one has

$$g(k) = k^2 - k\left[\frac{\overline{F} - (1-x)^2 v_f - x^2 v_g}{x(1-x)v_f}\right] + \frac{v_g}{v_f} = 0 \quad (3)$$

where

$$\overline{F} = \frac{F + A_e(P_R - P_e)}{AG^2/g_c} \quad (4)$$

It is necessary to write an expression for the stagnation energy balance in separated flow form:

$$H_0 = xh_g + (1-x)h_f + \frac{1}{2g_cJ}[xu_g^2 + (1-x)u_f^2] \quad (5)$$

and solve Equations (3) and (5) simultaneously in order to obtain values for slip ratio and quality. These were solved numerically using a modified Newton-Raphson technique (*15*).

The thrust exerted on the impulse cage was transmitted by a pendulum arrangement to a BLH type (3PIH) bonded strain gauge, single-bridge precision load cell. The cell was temperature compensated to 450°F. and calibrated to achieve ± 0.10% of full scale accuracy under operating conditions. Initially operation of the equipment resulted in unequal pressures between the plenum chamber and the hermetically sealed load cell container. In order to eliminate this additional force, a nitrogen pressure equilization system was installed between load cell and plenum chamber. Electrical output from the load cell was measured with a precision potentiometer.

EXPERIMENTAL RESULTS

Interest in this investigation centered on the dependence of critical flow rate on flow patterns and measured slip ratio and their dependence in turn on pressure gradients and quality. Experimental variable ranges were:

Choking mass velocity G_c	142 to 908 lb./(sq.ft.)(sec.)
Exit quality X_e	0.99 to 0.01
Exit pressure P_e	27.7 to 75.3 lb./sq.in.abs.
Exit slip ratio k_e	0.80 to 5.05
Exit flow pattern	Annular-mist to slug
Fluid medium	Steam-water

The variation in observed flow pattern is recorded on a Baker flow pattern chart shown in Figure 3. Previous investigators (*6, 7*) have calculated expected flow patterns based on Baker criterion, but this study apparently represents the first systematic record of visual observations of flow pattern under choking flow conditions. Variation of experimentally measured slip ratio with increasing pressure gradients at various quality levels examined is shown in Figure 7.

In order to evaluate experimental accuracy of this study, the maximum indeterminate error in directly measured quantities was estimated and used to calculate the error in the indirectly measured dependent variables, slip ratio and quality. The results are shown in Table 1 for representative high and low quality runs. For both low and high qualities, the largest error is seen to arise from errors in exit plane pressure determination. The formulation error inherent in assuming that a separated model can be used to describe choking flow obviously depends on how well the model describes experimentally observed behavior and will be discussed in subsequent sections.

FLOW REGIMES

The Baker flow regime chart used in Figure 3 is an empirically defined but surprisingly general map describing how the two phases of a liquid-gas system flowing through a pipe will distribute themselves with respect to one another as density, viscosity, surface tension, and flow rate parameters vary. [Note that mass velocities G and L have the dimensions of lb.$_m$/(sq.ft.)(hr.) in Figure 3 only.]

Visually observed flow patterns are subjective but very descriptive quantities which can aid in model building. Those reported for the various regimes of this study were found by visually observing the exit plane and free jet downstream of the exit.

The flow conditions used in this study corresponded to Baker chart flow regimes varying from dispersed to bubble or froth flow as quality was decreased. At the extreme left-hand portion of the curve representative of a 95% quality, the blue color of a 90-deg. side-illuminated jet indicated that the dispersed phase consisted of droplets in the 10^{-3} μ size range and no liquid film was observed. At lower qualities a thin film of liquid could be seen

TABLE 1. EFFECT OF INDEPENDENT VARIABLES ON SLIP RATIO AND QUALITY RESULTS

Variable	Measured value	Maximum variation	Slip ratio variation	Quality variation
	Run 19—High quality			
k	1.335			
x	0.7170			
F, lb.$_f$	11.455	±1.2%	±6.65%	±0.17%
H_0, B.t.u./lb.$_m$	945.73	±0.2%	±1.28%	±0.26%
w_g, lb./min.	11.00	±0.5%	±1.66%	±0.01%
w_f, lb./min.	3.23	±0.8%	±2.84%	±0.02%
P_E, lb./sq.in.abs. (centered probe)	30.17	+3.0%	−4.19%	+0.12%
P_E, lb./sq.in.abs. (extrapolation includes tap 1)	30.17	−11.4%	+27.20%	−0.60%
	Run 23—Low quality			
k	3.930			
x	0.0463			
F, lb.$_f$	4.578	±1.2%	±2.39%	±0.03%
H_0, B.t.u./lb.$_m$	701.07	±0.2%	±1.22%	±0.87%
w_g, lb./min.	11.73	±0.5%	±1.70%	0
w_f, lb./min.	46.66	±0.8%	±0.30%	0
P_E, lb./sq.in.abs. (centered probe)	27.77	0	0	0
P_E, lb./sq.in.abs. (extrapolation includes tap 1)	27.77	−7.94%	+11.50%	+10.24%

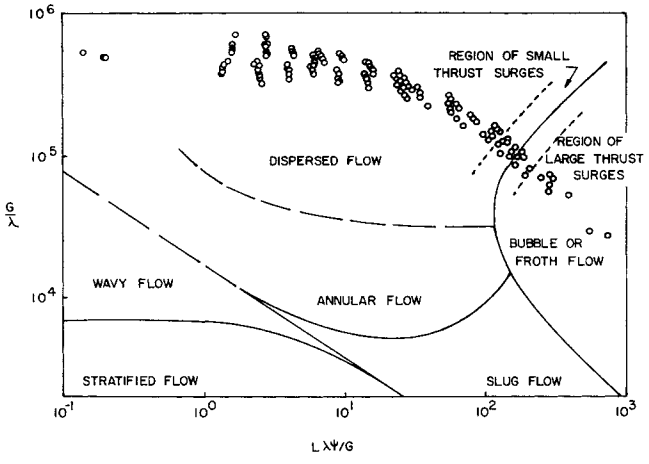

Fig. 3. Baker flow pattern chart.

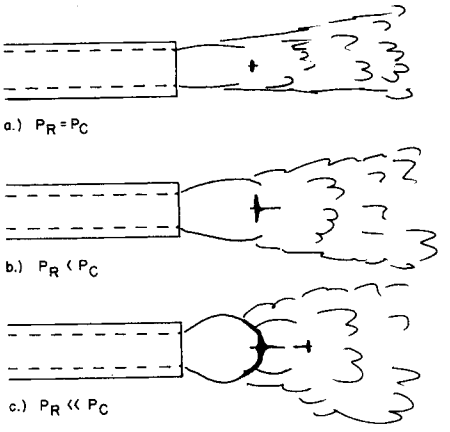

Fig. 4. Free jet appearance.

breaking off the inner walls of the end of the test section and the droplet size and population were seen to increase. As conditions corresponding to the so-called bubble or froth flow region were approached, the flow gradually took on a pulsing character. This gradual transition from one flow regime to another does not contradict Baker chart predictions since the limits of the Baker chart were never meant to be precise boundaries. However, the character of the new regime appeared to be more of an entrained-slug regime rather than a bubbly one. The generally accepted difference between the two is that gas bubbles in the slug-flow regime have grown to occupy the entire cross section of the pipe. The difference in behavior is due to the extreme pressure gradient existing near the end of the test section which results in any vapor slug exploding once it leaves the test section with considerable breakup of surrounding liquid. At the lowest qualities the visual impression was one of alternating cylinders of liquid and huge misty plumes of vapor.

Of particular interest was the observation that a condensation shock front was visible in the free jet. At high qualities the shock region initially occupied a small disclike region at the center of the jet approximately two tube diameters downstream of the end of the test section. As the pressure drop across the test section was increased, the shock front occupied a progressively larger fraction of the jet cross-sectional area. The small shock disc appeared at the point where little further change in pressure profile occurred within the test section and it grew to occupy the entire cross section when the pressure drop beyond the test section was approximately 30 lb./sq.in. The highest (95%) quality runs also produced a second shock front four diameters downstream of the exit plant at very low chamber pressures. At lower qualities the single shock front was less distinct visually but its axial position did not shift either with decreasing quality or with increasing pressure drop. Below a quality of about 30% the front could no longer be seen. Figure 4 indicates the general change in appearance of the free jet and the shock front as receiver pressure was lowered.

FREE JET PRESSURE PROFILES

Pressure probe 1 was used to measure static pressure in the expanding two-phase jet downstream of the exit as well as to explore the upstream profiles. Analysis of the free jet pressure measurements revealed the existence of standing prssure waves which increased in height with increasing pressure gradient and quality. Figure 5 illustrates the shape of the standing waves for two different qualities. Note how the standing waves are very small in the lower quality case. Faletti (*16*) reported similar waves and suggested that they resulted from the probe supports being used. The probe used in this study was built so no hardware interfered with the expanding free jet. Moreover, the existence of condensation fronts at the points of major pressure peaks indicated these were indeed shock waves. A compressible fluid initially flowing at subsonic velocities cannot be accelerated to supersonic velocities within a constant-diameter duct, but it is possible for a central core of fluid flowing from an underexpanded nozzle to accelerate to supersonic velocity in the region immediately downstream of the exit plane as the fluid expands. This fluid soon becomes unstable and shocks down to subsonic velocity. Fiedler (*17*) has studied shock wave formation in steam-water flow through converging-diverging nozzles and he observed that shock fronts were smeared out by the presence of droplets producing continuous pressure profiles similar to those observed in this study.

It is also of interest to note the discrepancy of wall tap pressure values and centered probe values as the exit plane is approached. These indicate that a radial pressure profile has been established. Such a difference was not noted at the 95% quality runs where no liquid film was observed. This suggested that the lower receiver pressure was transmitted upstream in the liquid film on the wall, giving an apparent radial gradient which in fact did not affect the essentially one-dimensional nature of the major flow. The extremely flat condensation shock disc supported this contention that the major flow was well described by a one-dimensional assumption.

Because the initial probe had a maximum positioning error of $\pm$ 0.005 in., a second probe was built to explore the question of radial pressure gradient. Some of the pressure profiles obtained with this probe are shown in Figure 6 for different quality levels. The continuous curves representing wall tap pressure values indicate that in the midquality range, the pressure taps near the end, including pressure tap 1 located 0.005 in. from the exit plane, gave readings which were more sensitive to receiver pressure than were the probe pressure values. On the other hand, at high qualities where no liquid film was observed and at low qualities where highly oscillatory slugging flow existed, the two types of pressure readings agreed quite well. This supported the hypothesis previously advanced that a reasonably stable, continuous liquid film existed in the midquality range (30 to 95%) transmitting a low receiver pressure further upstream. In the low quality region (< 30%) the flow was so unstable that no continuous path for transmittal through liquid phase existed. At

high quality (> 95%) no liquid film existed.

The value of measuring pressure in the core of the stream with a probe was that a check on the accuracy of extrapolation techniques could be obtained. Since the probe could not be used when thrust measurements were made, the relationship between wall extrapolations and the pressure existing in the bulk of the fluid had to be characterized before making ay thrust measurements. After examining the differences over the entire quality range studied, Figures 5 and 6, it was decided that the most accurate way of finding exit pressure was to continue to extrapolate from the wall tap 0.033 in. upstream of the exit because probe wall tap comparisons indicated this gave an almost exact match of pressures. This basic method has been used by earlier critical flow researchers, but the important difference is that maximum errors inherent in this method were quantified by comparison with probe results in this research. It was calculated that the maximum error in measured slip ratio was 4% using the pressure extrapolation procedure.

Since the probe pressure measurements were made with the thrust measuring cage removed, it was pertinent to see what effect the presence of the cage would have on pressure profiles both upstream and downstream of the exit. A fixed dummy cage was installed in place of the pendulum hung cage used for thrust measurement, and pressure probe 1 was traversed through it and up into the test section. The results demonstrated that no choking effects resulted from the presence of the cage and that the free jet pressure decayed essentially in the same manner whether the cage was present or not. Most important, the static pressure upstream and downstream of the flat backup plate on the momentum cage agreed exactly.

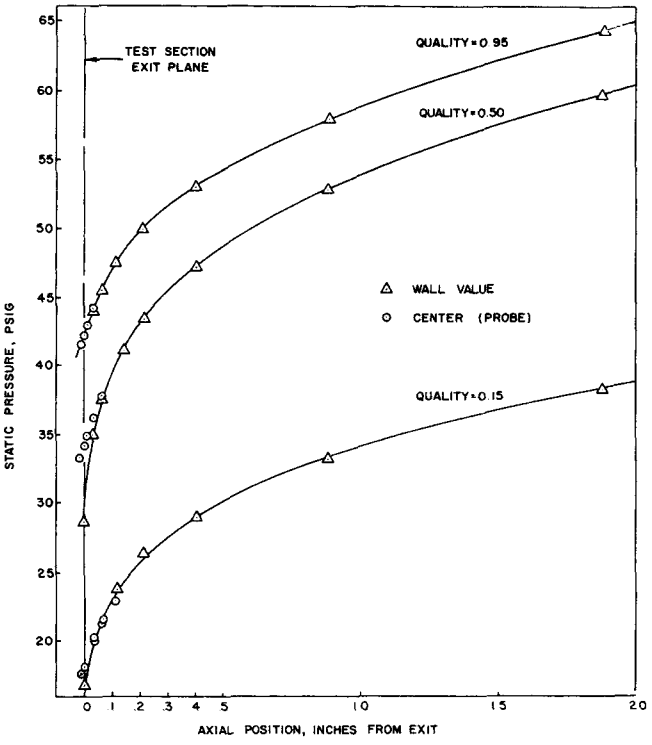

Fig. 6. Radial pressure profile.

SLIP RATIO

Slip ratios were measured for choked flow over a wide range of qualities. The velocity ratio was found by simultaneous evaluation of the force balance and stagnation energy balance, Equations (3) and (5). The resultant values of gas to liquid velocity ratio or slip ratio k are given in Figure 7, plotted versus homogeneous model quality. Quality determined from the above simultaneous system of equations is an implicit function of slip, so all plots were made in terms of homogeneous quality to eliminate the necessity of trial and error procedure for slip determination at a given quality.

The vertical progression of slip ratios at a particular quality is a result of the experimental technique used. A run was set up at a particular quality with the plenum chamber at its lowest possible pressure. Slip at critical flow obtained under these conditions is the largest value in a series. The back pressure was then raised in successive increments until a reduction from maximum or choking flow was observed. The incremental decreases in overall pressure drop also reduced the acceleration of vapor past liquid and resulted in lower slip ratio values. At low qualities the change in amount of evaporation with change in exit pressure produced greater spread in quality at a set upstream condition.

The eight data points of Lining (3) have been included in Figure 7 along with the experimental slip ratio correlation developed by Vance (6) for subcritical flows

$$K = 1.465 \left[\frac{1 - x_H}{x_H} \cdot \frac{G}{G_c} \right]^{0.3021} \qquad (6)$$

These data are the only experimental measurements of slip ratio for high-velocity conditions characteristic of choking flow. The general agreement with Vance's data is excellent, but the low quality results of Linning taken on a 0.120-in. diam test section are significantly higher. Flow in this low quality region is extremely unstable, so that

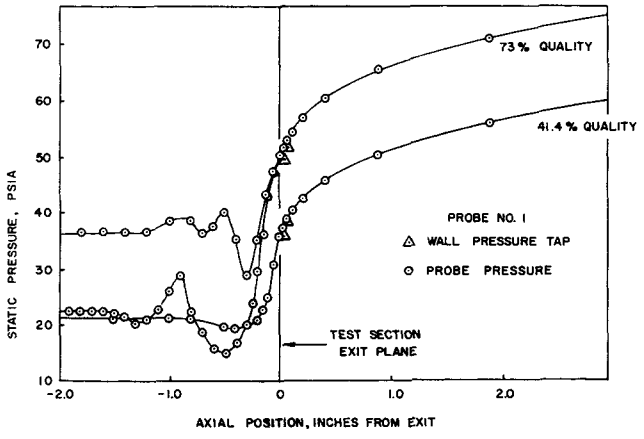

Fig. 5. Static pressure versus axial position.

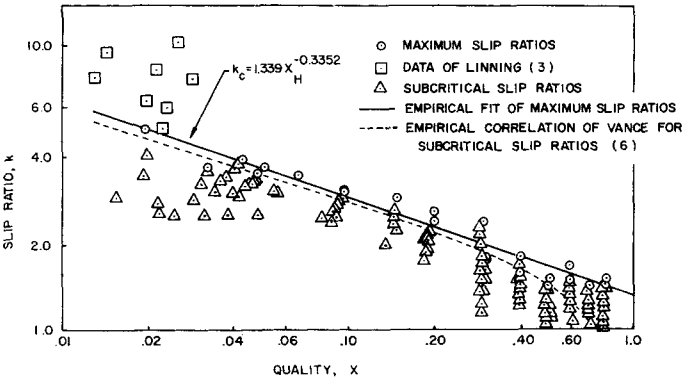

Fig. 7. Slip ratios.

Table 2. Slip Ratio Comparison—Model and Experiment

Exit pressure, lb.sq.in.abs.	Measured slip at qualities of 0.02	0.04	0.96	Model slip $(v_g/v_f)^{1/2}$	$(v_g/v_f)^{1/3}$
30	5.05	1.80	1.20	28.4	9.3
50	—	1.57	1.10	22.2	7.9

inertial effects in experimental equipment probably result in greater error in slip ratio determined on different experimental setups.

Of prime interest in this investigation was the magnitude of the maximum slip ratios obtained under choking conditions. Every effort was made to ensure that the slip ratio measured at the minimum plenum pressure represented a limiting or critical condition. The thrust value corrected for pressure loss in the receiver was experimentally verified to be an approximate maximum. In most cases, thrust was not strongly sensitive to plenum chamber pressure once fully developed critical flow existed. Exit pressure was also checked to make sure it was an essentially unchanging minimum.

The various analytical models recognize the asymptotic nature of flow choking and use it as a basis for deriving an explicit expression for the critical or limiting slip ratio. By developing different expressions for mass velocity in terms of the momentum or energy equations, these models require that in the limit slip ratio should be a function only of the thermodynamic properties of the two phases and equal either to the square root or the cube root of the ratio of vapor to liquid specific volumes (*1, 7, 10*). The range of measured values are compared to these model predictions in Table 2.

The experimental values clearly do not agree with model predictions. Not only are the measured critical flow slip ratios lower in absolute magnitude than the analytical models, they also exhibit a strong quality dependence not accounted for in any developments to date. An insufficient amount of data was taken over a broad pressure range to test rigorously the pressure dependence predicted by the specific volume ratio dependence of the models but the trends of experimental values do indicate that lower slip ratios result at higher exit plane pressure. If one considers the amount of entrainment of liquid as fine droplets observed in this study, it does not come as a surprise that measured slip ratios are less than predicted by a model which assumes no momentum interchange between phases other than through evaporation. At high qualities extremely fine liquid droplets were observed to be distributed uniformly throughout the jet cross section. As the quality decreased, the size of the liquid droplets increased and a fine liquid film was observed at the wall. This supports the experimental finding that slip ratio increased as quality decreased. The problem becomes one of determining if an analytical expression for slip ratio can be developed which accounts for liquid entrainment with little increase in model complexity.

To determine how serious the conceptual problem was, a simple, entrained-separated flow (ESF) model was developed. A vapor-phase momentum balance over a differential volume was developed:

$$-A_g dP = \frac{1}{g_c}\left[(w_g + dw_g)(u_g + du_g) - w_g u_g - Du_g dw_g - (1-D)u_f dw_g\right] \quad (7)$$

where a constant weight fraction D of the liquid is moving at the velocity of the vapor and a fraction $(1-D)$ is moving at the liquid velocity. The model assumes that evaporation is occurring from the entrained and nonentrained liquid in the same ratio as the weight distribution of the liquid itself. Similarly for the liquid phase

$$-A_f dP = \frac{1}{g_c}\left[(w_f + dw_f)(u_f + du_f)(1-D) + (w_f + dw_f)(u_g + du_g)D - (w_f u_f)(1-D) - (w_f u_g)D - (u_g dw_f)D - (u_f dw_f)(1-D)\right] \quad (8)$$

Upon further manipulation, detailed in reference *15*, one obtains an expression for critical flow:

$$G_c = \sqrt{-g_c\left(\frac{dP}{dV_E}\right)} \quad (9)$$

where the expression for volume of an entrained-separated system is

$$V_E = \frac{v_g(x^2 + Dx(1-x))}{\alpha} + \frac{v_f(1-x)^2(1-D)^2}{(1-\alpha)\left[1 - D\left(\frac{v_f}{v_g}\right)\left(\frac{1-x}{x}\right)\left(\frac{\alpha}{1-\alpha}\right)\right]} \quad (10)$$

The expression for critical slip ratio of the ESF model is obtained by differentiating the ESF expression for kinetic energy with respect to void fraction or slip ratio. The result

$$k = D + (1-D)\left(\frac{v_g}{v_f}\right)^{1/3}\left[\frac{1 + D\left(\frac{v_g}{v_f}\right)\left(\frac{1-x}{x}\right)}{1 + D\left(\frac{1-x}{x}\right)}\right]^{1/3} \quad (11)$$

is based on the assumption that choking involves minimization of entropy production as monitored by kinetic energy (*11*). Equation (11) has been plotted on Figure 8 along with measured values of slip ratio for entrainment fractions ranging from complete entrainment ($D = 1$, that is, all liquid moving at the vapor velocity) which corresponds to the homogeneous model to zero entrainment ($D = 0$) which corresponds to the regular separated flow model.

The simple entrained model predictions of slip were compared with experimental values to determine how the fraction entrained D varied with quality. Values of D were estimated at each experimental point in Figure 8 and the results plotted versus quality in Figure 9. (No experimental measurement of D was made.) There seem to be two distinct regions on the plot with the break point around 25% quality. This transition point corresponds to the visually observed change in flow regime from dispersed-annular to entrained slug flow. The values of the entrainment fraction found by the above method were approximated by two linear functions of logarithm of quality:

$$D = 1.0 + 0.140 \ln(x) \quad \text{for } 1.0 < x < 0.25 \quad (12)$$

$$D = 0.94 + 0.204 \ln(x) \quad \text{for } 0.25 < x < 0.01 \quad (13)$$

When these equations were substituted back into Equation (11) empirical slip values were obtained which agreed

with the experimentally measured slip ratios with an average error of 7.8% and a maximum deviation of 26.7%.

CRITICAL FLOW RATES

Critical flow rates measured in this research at 30 and 50 lb./sq.in.abs. are shown in Figure 10 where the logarithm of critical flow rates is plotted versus quality. The experimental values agree well with earlier data of Zaloudek (*4*), Cruver (*7*), and Faletti (*16*), except for the latter's reported secondary maximum in critical flow ratio at about 10% quality.

The success of the derived ESF model is tested graphically in Figure 10. Since a separate quantitative determination of entrainment was not made in this research, the model is presented in general form at two limiting levels of entrainment (0 and 100% entrainment of water droplets at steam velocity). By varying the value of D, the experimental flow rates below 10% quality can be predicted quite closely. However, the values of D necessary to fit the flow rate curves are far higher than those necessary to fit slip ratio data. The entrained model has value in illustrating the effect of entrainment on critical flow rates, however, it does not appear to have quantitative value in predicting critical flow rates.

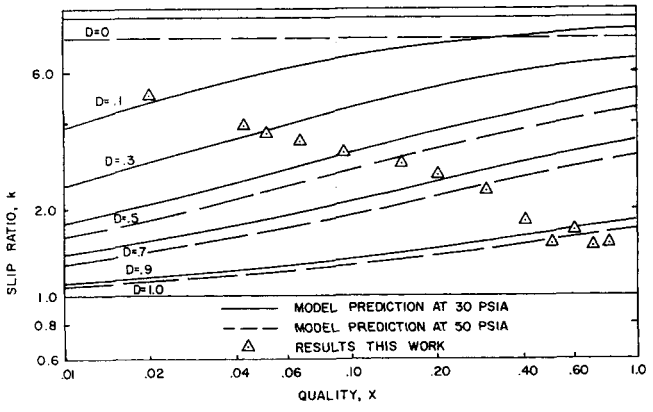

Fig. 8. Slip ratio versus ESF model.

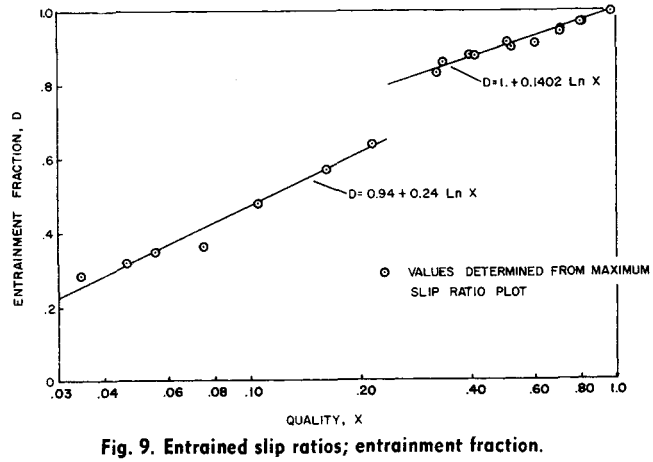

Fig. 9. Entrained slip ratios; entrainment fraction.

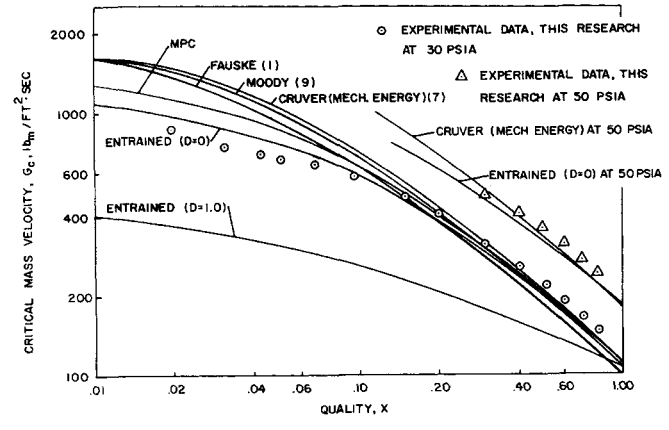

Fig. 10. Critical flow rates.

Because of the generally marginal performance of these two models, it was considered timely to compare several other currently used models of critical flow. Figure 10 also compares the models of Cruver (*7*), Fauske (*1*), Levy (*8*), Moody (*9*), and the models derived in this research. In comparing these models it was noted that none accounted for the fact that condensation rather than vaporization is the result of a high quality isentropic expansion. To correct for this a new analytical model was derived (*15*), the monitored phase change (MPC) model, which accounted for the net phase change over the entire quality range. However, as can be seen in Figure 10, the MPC model produced only a slight improvement in model predictive accuracy at higher qualities. It was concluded that no one analytical model was broadly applicable. They all predict flow rates which are 10 to 15% below experimental results at high qualities. Below a quality of 10% no one model is really very accurate, although as has been pointed out empirical variation of the entrainment fraction D could be used to fit the data.

Sharp criticism of the analytical techniques employed in deriving these models hardly seems justified in view of the marginal success any of them exhibit in describing experimental results. If the general separated flow model approach is to be continued, separate methods must be developed for determining average values of slip, entrainment, and metastability in a single experiment.

AN EMPIRICAL MODEL

Because none of the analytical models was entirely satisfactory, an empirical means was sought to correlate the results. Faletti (*16*) derived an empirical expression which has been quite satisfactory in predicting results down to 20% quality. Means were sought for developing a more phenomenologically based model incorporating the notions of both slip and entrainment into a model which could be presented in closed form and would cover a much broader quality range.

The method developed involves calculating critical flow rate from the energy balance

$$G_c = \left\{ \frac{2g_c J(H_0 - h_f - xh_{fg})}{\left[\frac{xv_g}{k} + (1-x)v_f\right]^2 [1 + x(k^2 - 1)]} \right\}^{1/2} \tag{14}$$

where slip ratios were obtained from expression (11) and values of the entrainment fraction D were obtained from the graphically developed empirical relations (12) and (13). The enthalpy and specific volume terms were evaluated at critical exit pressure using either appropriate Mollier diagrams or least square fits of published data (*15*). Quality was calculated using Equations (3) and (5), although use of homogeneous quality introduced an error of less than 1% over the entire range considered. Substituting the empirically developed relationship for entrainment sensitive slip ratio into (14) resulted in values for critical mass velocity which agreed with measured

values with an average error of less than 2%. This method of calculating critical flow rates is recommended for use over the quality range of 0.01 to 0.99 and pressure range of 20 to 75 lb./sq.in.abs. Its accuracy beyond these ranges has yet to be established.

SUMMARY

The following conclusions can be drawn as a result of this research:

1. A critical or minimum pressure was measured at the exit plane of a duct in which a two-phase, one-component mixture is flowing under choked conditions. Supersonic flow with accompanying shock down was observed in the potential core of the free jet downstream of the duct exit plane at qualities above 25%. The cross-sectional area of the normal shock front was observed to grow as the plenum chamber pressure was reduced below the critical exit plane pressure.

2. Three separate flow regimes were observed in this research. At qualities above 95% an entrained flow pattern was observed. Between 95 and 25% quality increasing amounts of liquid were observed on the wall of the test section along with increasing diameter liquid droplets. This was classified as an annular-entrained flow regime. At qualities below 25% the flow became increasingly irregular and was dubbed an entrained slug-flow regime. These regions were entered into the Baker flow chart.

3. Slip ratios were measured at critical flow. The values did not agree with previous separated flow model predictions. Both entrainment and metastability are seen as reasons for the lack of agreement.

4. Critical flow rates were measured which agreed experimentally with results of previous investigators.

5. Two new phenomenologically based models for critical flow of two-phase, one-component mixtures were derived. One accounted for the fact that net condensation is the result of a high quality expanding flow. The second took into account the fact that some mass fraction of the liquid was entrained as droplets moving at the velocity of the vapor stream. Neither model offered a major improvement over existing phenomenological models.

6. An accurate critical flow model was developed based on an empirical correlation of critical slip ratios as a function of quality. This semiempirical model offers a major improvement in broad applicability and accuracy over existing models.

ACKNOWLEDGMENT

The authors thank the U.S. Atomic Energy Commission and the National Science Foundation for support of the experimental work. Financial support for W. J. Klingebiel in the form of research assistantships by the Atomic Energy Commission and the Engineering Experiment Station of the State of Washington, an instructorship provided by the Department of Chemical Engineering of the University of Washington, and a fellowship provided by the National Science Foundation were greatly appreciated.

NOTATION

A = cross-sectional area for flow, sq.ft.
D = weight fraction of liquid entrained at vapor velocity
d = diameter of conduit, ft.
F = thrust measured by load cell, lb.$_f$
$\overline{F}$ = momentum force of flowing fluid, lb.$_f$
F_i = frictional dissipation, lb.$_f$
G = mass velocity, lb.$_m$/(sq.ft.)(sec.)
g_c = conversion factor, 32.174 ft. lb.$_m$/(lb.$_f$) (sec.^{2})
H, h = enthalpy, B.t.u./lb.$_m$
J = conversion factor, 778.16 ft. lb.$_f$/B.t.u.
k = slip ratio, u_g/u_f
L = distance, ft.
P = pressure, lb./sq.in.abs.
S = entropy, B.t.u./(lb.$_m$)(°F.)
T = temperature, °F.
u = average velocity, ft./sec.
v = specific volume, cu.ft./lb.$_m$
W, w = mass flow rate, lb.$_m$/sec.
x = quality

Greek Letters

α = void fraction
β = ratio of vapor to liquid specific volumes
$\lambda = \left[\left(\frac{\rho_g}{0.075}\right)\left(\frac{\rho_f}{62.3}\right)\right]^{1/2}$
μ = fluid viscosity, lb.$_m$/(ft.)(sec.)
ν = liquid surface tension, dynes/cm.
ρ = density, lb.$_m$/cu.ft.
$\psi = \left(\frac{73}{\nu}\right)\left[\mu_f\left(\frac{62.3}{\rho_f}\right)^2\right]^{1/3}$

Subscripts

c = critical flow conditions
E = entrained model average specific volume
e = exit plane of test section; or exit from experimental equipment
f = liquid phase
fg = change from vapor to liquid phase
g = vapor phase
H = homogeneous model
m = separated model average specific volume
R = receiver chamber
0 = stagnation conditions

LITERATURE CITED

1. Fauske, H. K., *U.S. Atomic Energy Comm. Doc. ANL-6633* (1963).
2. Isbin, H. S., J. E. Moy, and A. J. R. Cruz, *AIChE J.*, **3**, 361 (1957).
3. Linning, D. L., *Proc. Inst. Mech. Engr. (London)*, **1B** (2), 64 (1952).
4. Zaloudek, F. R., *U.S. Atomic Energy Comm. Doc. HW-68934* (1961).
5. Smith, R. V., *NBS-TN-179* (Aug 1963).
6. Vance, W. H., and R. W. Moulton, *AIChE J.*, **11**, 1114 (1965).
7. Cruver, J. E., Ph.D. thesis, Univ. Washington, Seattle (1963).
8. Levy, Sol, *General Electric Co. Rept. GEAP-4395* (Oct. 1963).
9. Moody, F. J., *General Electric Rept. APED-4378* (Oct. 1963).
10. Zivi, S. M., *Trans. A.S.M.E. J. Heat Transfer*, **86-C**, 247 (1964).
11. Prigogine, I., "Introduction to Thermodynamics of Irreversible Processes," 2nd edit., Interscience, New York (1961).
12. Hatch, M. R., and R. B. Jacobs, *AIChE J.*, **8**, 18 (1962).
13. Ryley, D. J., *Engineer (London)*, **143**, 332 (1952).
14. Chu, B. T., *"Proc. 1958 Heat Transfer and Fluid Mech. Inst.,"* Stanford Univ. Press, Stanford, Calif. (1958).
15. Klingebiel, W. J., Ph.D. thesis, Univ. Washington, Seattle (1964).
16. Faletti, D. W., and R. W. Moulton, *AIChE J.*, **9**, 247 (1963).
17. Fiedler, R. A., *U.S. Atomic Energy Comm. Doc. UCRL-6676* (1961).

Manuscript received March 10, 1969; revision received February 9, 1970; paper accepted February 13, 1970. Paper presented at AIChE Portland meeting.